Process contributions of Australian ecosystems to interannual variations in the carbon cycle

2016 Environ. Res. Lett. 11 054013

(http://iopscience.iop.org/1748-9326/11/5/054013)

Environmental Research Letters

LETTER

Process contributions of Australian ecosystems to interannual variations in the carbon cycle

Vanessa Haverd[1,4], **Benjamin Smith**[2] **and Cathy Trudinger**[3]

[1] CSIRO Oceans and Atmosphere, GPO Box 3023, Canberra ACT 2601, Australia
[2] Lund University, Department of Physical Geography and Ecosystem Science, SE-22362 Lund, Sweden
[3] CSIRO Oceans and Atmosphere, PMB 1 Aspendale, Vic 3195, Australia
[4] Author to whom any correspondence should be addressed.

E-mail: vanessa.haverd@csiro.au

Keywords: global carbon cycle, semi-arid ecosystems, Australia, interannual variability, net carbon uptake, net primary production, precipitation anomalies

OPEN ACCESS

RECEIVED
4 January 2016

REVISED
18 April 2016

ACCEPTED FOR PUBLICATION
26 April 2016

PUBLISHED
10 May 2016

Abstract

New evidence is emerging that semi-arid ecosystems dominate interannual variability (IAV) of the global carbon cycle, largely via fluctuating water availability associated with El Niño/Southern Oscillation. Recent evidence from global terrestrial biosphere modelling and satellite-based inversion of atmospheric CO_2 point to a large role of Australian ecosystems in global carbon cycle variability, including a large contribution from Australia to the record land sink of 2011. However the specific mechanisms governing this variability, and their bioclimatic distribution within Australia, have not been identified. Here we provide a regional assessment, based on best available observational data, of IAV in the Australian terrestrial carbon cycle and the role of Australia in the record land sink anomaly of 2011. We find that IAV in Australian net carbon uptake is dominated by semi-arid ecosystems in the east of the continent, whereas the 2011 anomaly was more uniformly spread across most of the continent. Further, and in contrast to global modelling results suggesting that IAV in Australian net carbon uptake is amplified by lags between production and decomposition, we find that, at continental scale, annual variations in production are dampened by annual variations in decomposition, with both fluxes responding positively to precipitation anomalies.

1. Introduction

There is compelling new evidence of the important role of semi-arid ecosystems in the variability of the global carbon cycle. In a regional attribution of terrestrial biosphere model predictions of global net biome productivity (NBP), Ahlström *et al* (2015) demonstrated that, while tropical forests dominate the mean of global NBP (1982–2011), semi-arid ecosystems dominate both its interannual variability (IAV) and trend. The same study found that in semi-arid ecosystems, IAV in modelled NBP is dominated by the response of vegetation productivity to variations in water availability, strongly associated with the El Niño/Southern Oscillation (ENSO). ENSO explains more than 40% of global net primary production (NPP) variability, mainly driven by the response of Southern Hemisphere ecosystems, particularly in tropical and subtropical regions (Bastos *et al* 2013). The large role of semi-arid ecosystems in global carbon uptake anomalies is further exemplified by the significant contribution of Australia, the driest inhabited continent, to the record residual global land sink of 2011 of 1.5 ± 0.9 $[1\sigma]$ PgC yr^{-1} relative to the 2003–2012 decadal mean (Le Quéré *et al* 2015). Haverd *et al* (2013a) quantified a 2011 Australian land sink anomaly (relative to 1990–2011) of 0.5 PgC, based on a biogeochemical land surface model applied to Australia and constrained by multiple regional observations. Using the global LPJ model, Poulter *et al* (2014) inferred that Australian ecosystems contributed a similar 2011 sink anomaly (relative to 2003–2012) of 0.70 PgC, with other large positive contributions from Africa (0.45 PgC), South America (0.26 PgC) and Tropical Asia (0.13 PgC). By inversion of satellite-derived atmospheric CO_2 observations,

Detmers *et al* (2015) also inferred a large Australian land sink in 2011 (0.79 PgC).

These earlier studies point out that 2011 was an exceptional year in terms of the regional climate and its effects on ecosystem functioning, but the specific climatic drivers and responding mechanisms have not been clearly identified. In this work we upscale carbon and water fluxes from 14 sites of the OzFlux network (Isaac 2014) using a biogeochemical land surface model further constrained by observations of biomass, soil carbon, streamflow and remotely sensed vegetation cover (Zhu *et al* 2013) (updated from Haverd *et al* 2013b). We use the results to quantify IAV in the Australian terrestrial carbon cycle, including the magnitude of the 2011 anomaly, and go on to attribute the IAV and its major component fluxes spatially and to responding processes.

2. Methods

Australian net ecosystem productivity (NEP) (1982–2013) and its components, R_H and NPP, were derived using model-data synthesis (Trudinger *et al* 2016), updated from (Haverd *et al* 2013a), the only published assessments of Australian biospheric carbon balance which integrate multiple regional observation sources. Of these sources, remotely sensed vegetation cover and flux-tower observations of carbon and water exchange are particularly relevant constraints on interannual variations. Evaluation metrics (Trudinger *et al* 2016) reveal good prediction of OzFlux annual gross primary production ($n = 70$, $r^2 = 0.63$, normalised root mean squared error $\sqrt{\overline{(y-x)^2}}/\sigma_x$, NRMSE = 0.4), with poor correlation but acceptable variance in NEP ($n = 70, r^2 = 0.01$, NRMSE = 1.1).

The model-data synthesis is described briefly below: full details are provided by Haverd *et al* (2013a) and Trudinger *et al* (2016). The synthesis employs BIOS2, a fine-spatial-resolution (0.05°) offline modelling environment, including a modification of the CABLE biogeochemical land surface model (Wang *et al* 2010, 2011b) incorporating the SLI soil model (Haverd and Cuntz 2010). BIOS2 parameters are constrained and predictions are evaluated using multiple observation sets from across the Australian continent, including streamflow from 416 gauged catchments, eddy flux data (CO_2 and H_2O) from 14 OzFlux sites (Isaac 2014), litterfall data, and soil, litter and biomass carbon pools.

CABLE consists of five components (Wang *et al* 2011a): (1) the radiation module describes direct and diffuse radiation transfer and absorption by sunlit and shaded leaves; (2) the canopy micrometeorology module describes the surface roughness length, zero-plane displacement height, and aerodynamic conductance from the reference height to the air within canopy or to the soil surface; (3) the canopy module includes the coupled energy balance, transpiration, stomatal conductance and photosynthesis of sunlit and shaded leaves; (4) the soil module describes heat and water fluxes within soil and snow at their respective surfaces; and (5) the ecosystem carbon module accounts for the respiration of stem, root and soil organic carbon decomposition. In BIOS2, the default CABLE v1.4 soil and carbon modules were replaced respectively by the SLI soil model (Haverd and Cuntz 2010) and the CASA-CNP biogeochemical model (Wang *et al* 2010). Modifications to CABLE, SLI and CASA-CNP for use in BIOS2 are detailed in (Haverd *et al* 2013a).

Parameter estimation is achieved using the Levenberg–Marquardt method, as implemented in the PEST software (Doherty *et al* 2010) to minimise residuals between predictions and observations. An ensemble of parameter sets that are consistent with the observations are generated using the null space Monte Carlo method (Doherty *et al* 2010). Variance of predictions based on this ensemble of parameter sets is equated with variance attributable to parameter equifinality in model predictions.

Vegetation cover is prescribed, using a monthly time series of fractional absorbed photosynthetically active radiation (fPAR) for January 1982 to December 2013 that was derived from the third generation (NDVI3g) of the Global Inventory Modeling and Mapping Studies' normalised difference vegetation index (NDVI) time series (Tucker *et al* 2005, Zhu *et al* 2013). A monthly maximum composite was created from the original 15 day series, and the data were resampled from the original 0.0833° resolution (8 km) to 0.05° (5 km). NDVI values from 0.1 (bare ground) to 0.75 (full cover) were linearly rescaled between 0 and 1 to represent vegetation fractional cover. Total fPAR is partitioned into persistent (mainly woody) and recurrent (mainly grassy) vegetation components, following the methodology of Donohue *et al* (2009) and Lu *et al* (2003). This methodology takes advantage of low levels of seasonal change in LAI in woody vegetation, allowing seasonal variation in fPAR to be attributed principally to grassy vegetation. The remaining and relatively constant fPAR signal is attributed to woody vegetation. LAI for woody and grassy components are estimated by Beer's Law (e.g. Houldcroft *et al* 2009):

$$\mathrm{LAI}_W = -\frac{1}{k}\log_e(1 - \mathrm{fPAR}_W), \quad (1)$$

$$\mathrm{LAI}_G = -\frac{1}{k}\log_e\left(1 - \frac{\mathrm{fPAR}_G}{1 - \mathrm{fPAR}_W}\right), \quad (2)$$

where the vegetation type is either W (persistent or mainly woody) or G (recurrent or mainly grassy) and k is an extinction coefficient, set here to 0.5. In contrast to earlier BIOS2 simulations (Haverd *et al* 2013a), equation (2) accounts for the effect of shading of grass by woody vegetation.

We partition flux variability amongst component fluxes (components may be spatial or process

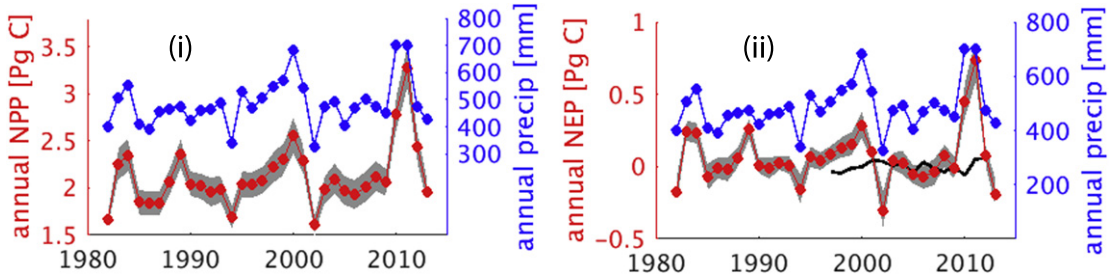

Figure 1. Australian continental annual net primary production (NPP) (i) and net ecosystem production (NEP) (2015) (ii) (red) and precipitation (blue). Grey shading represents the 2σ uncertainty associated with parameter equifinality. The solid black line (left axis) represents gross continental fire emission anomalies from GFED4 (Updated from van der Werf *et al* 2010).

contributions) using the formalism of Ahlström *et al* (2015) (equation (3))

$$f_j = \frac{\sum_t \frac{x_{jt}\,|X_t|}{X_t}}{\sum_t |X_t|}. \qquad (3)$$

Here x_{jt} is the flux anomaly (departure from a long-term trend) for the jth constituent flux at time t (in years), and X_t is the total flux anomaly, with $X_t = \sum_t x_{jt}$. By this definition, the jth contribution to the total IAV, f_j, is the average relative anomaly x_{jt}/X_t for the jth constituent, weighted with the absolute global anomaly $|Xt|$. The definition ensures that $\sum_j f_j = 1$, but allows individual contributions to fall outside the range (0, 1) if the total anomaly X_t arises from partially cancelling contributions x_{jt} from different constituents.

We focus on IAV in NEP, which is the difference between NPP and heterotrophic respiration (R_H), in the absence of disturbance. We do not account here for the component of IAV in NBP attributable to disturbance (land use and natural disturbance agents, mainly fire): the IAV of gross Australian fire emissions (based on the Global Fire Emissions Database (GFED3); van der Werf *et al* 2010) is less than 20% of IAV in Australian NEP (Haverd *et al* 2013b), while global modelling studies suggest that the net contribution of wildfires to semi-arid ecosystem IAV is small (Ahlström *et al* 2015). We confirm this by presenting updated gross annual fire emission anomalies (GFED4s) (udated from van der Werf *et al* 2010) alongside our estimated NEP anomalies.

3. IAV in Australian vegetation productivity and net carbon uptake

Figure 1 shows the time series of annual precipitation, NPP and NEP for the Australian continent, as estimated using BIOS2. Uncertainty on the NPP and NEP estimates represents 2σ variability attributable to model parameter equifinality. The time series is restricted to 1982–2013, as this is the period of data availability for the vegetation cover inputs.

IAV in NPP is 0.3 PgC yr^{-1} [1σ] or 15% of the mean flux. Temporal correlation between production and decomposition reduces the amplitude of IAV in NEP to 0.2 PgC yr^{-1} [1σ] or 10% of mean NPP. By contrast, IAV in gross continental fire emissions is only 0.04 PgC yr^{-1} [1σ], or 2% of mean NPP.

Highly anomalous values of NPP and NEP occur in 2011, the second of two consecutive years of very high rainfall. For comparison with the global residual land sink, we calculate anomalies for 2011 relative to the 2003–2012 period. The data in figure 1 give NPP, R_H and fire anomalies of 1.0 ± 0.2 [2σ], 0.42 ± 0.2 [2σ] and 0.05 PgC respectively. These may be compared with corresponding respective values of 0.79, 0.13 and −0.04 PgC in the analysis by Poulter *et al* (2014). Thus our estimated NEP anomaly of 0.6 ± 0.2 [2σ] PgC accounts for 40% of the record global land sink anomaly and agrees well with the NEP flux anomaly (NPP minus R_H) (0.66 PgC) from Poulter's analysis. However the component flux anomalies (NPP and R_H) are quite different in our study compared with Poulter *et al* suggesting that heterotrophic respiration is less responsive to high water availability in the global LPJ model than in BIOS2. Further, fire emissions, while small, are of opposite signs in the two analyses, pointing to a significant discrepancy between Australian fire emissions from GFED and from the global LPJ model.

4. Spatial attribution of IAV of continental net carbon uptake and its component fluxes

For the purpose of regional attribution, we use the bioclimatic classification of figure 2(i) which is an aggregation of classes from the agro-climatic classification of Hutchinson *et al* (2005) (table 2, figure 3). Australian biogeography strongly reflects rainfall pattern (figure 2(ii)). The contributions (equation (1)) of the ecosystems of each region to IAV in continental NPP, R_H and NEP are shown in figure 2(iii). The Sparsely Vegetated and Savanna regions dominate contributions to continental inter-annual variability in all three fluxes, together representing a 90% contribution to IAV in continental NEP. Notably, the

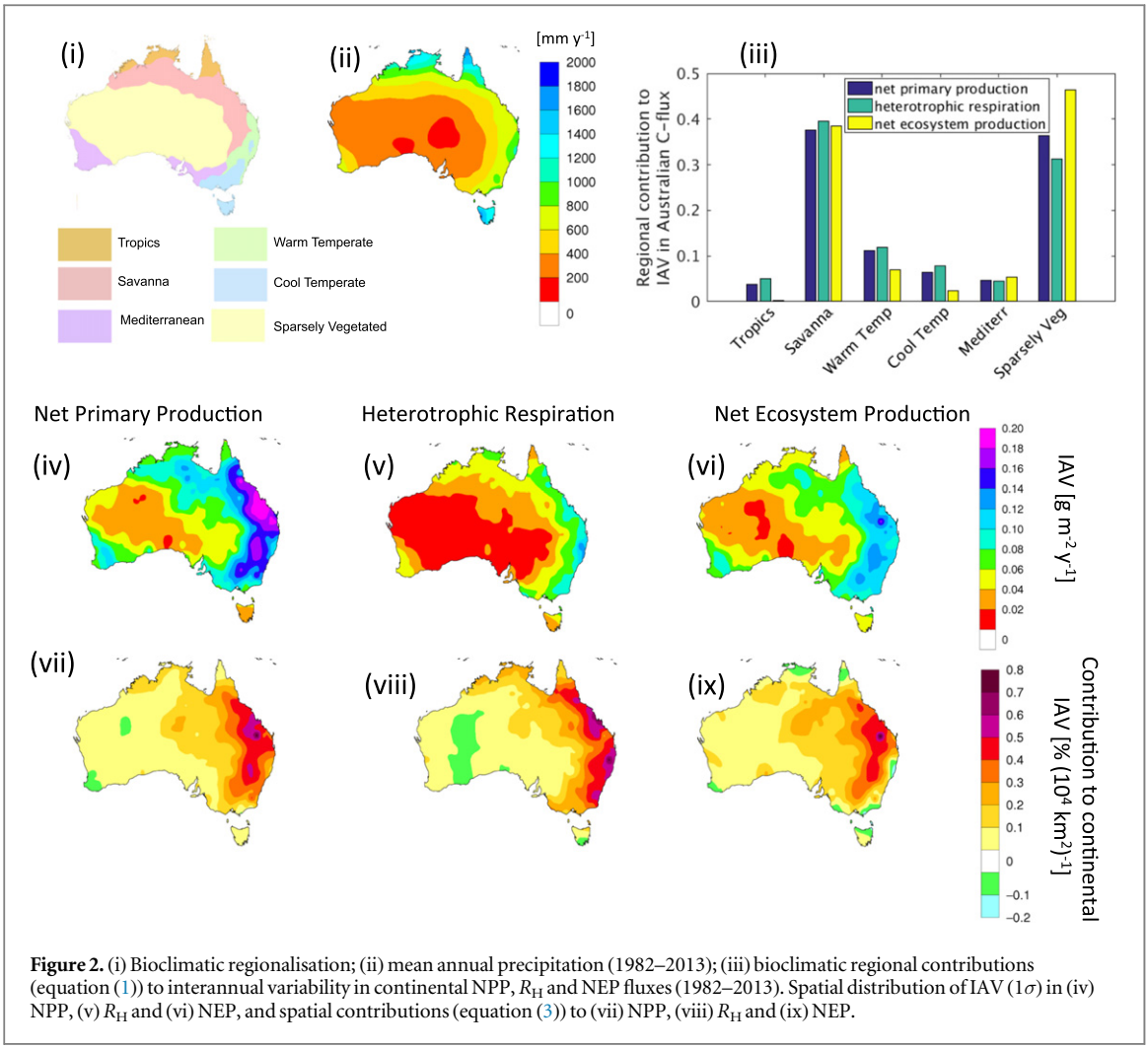

Figure 2. (i) Bioclimatic regionalisation; (ii) mean annual precipitation (1982–2013); (iii) bioclimatic regional contributions (equation (1)) to interannual variability in continental NPP, R_H and NEP fluxes (1982–2013). Spatial distribution of IAV (1σ) in (iv) NPP, (v) R_H and (vi) NEP, and spatial contributions (equation (3)) to (vii) NPP, (viii) R_H and (ix) NEP.

Sparsely Vegetated inland region, which contributes 36% to IAV in continental NPP, has a much larger contribution of 46% to variability in continental NEP, a result we will explore further in section 6 when we quantify process contributions to IAV in NEP.

Figures 2(iv)–(ix) shows the spatial distribution of IAV in NPP, R_H and NEP fluxes, and the spatial contributions to IAV in the continental fluxes. At the annual time-scale, NPP is most variable across the eastern part of the savanna belt (figure 2(iv)), a region of highly variable rainfall where vegetation is both productive and strongly responsive to water availability (Raupach *et al* 2013). Variability of heterotrophic respiration (figure 2(v)) is high along the eastern seaboard where high labile carbon stores coincide with high variability in soil moisture availability. The variability in NEP (figure 2(vi)) is lower overall than the constituent fluxes and with a spatial distribution reflecting elements of both components. The spatial contribution maps (figures 2(vii)–(ix)) contrast with the maps of IAV because of spatial differences in the timing of the variability. For example, significant IAV in C fluxes in the South–West of Western Australia contribute negligibly to continental IAV, suggesting that the variability in this region is not correlated with that of the continent as a whole, a pattern also evident for the precipitation driver (not shown), and related to the dominant influence of the Indian Ocean Dipole on rainfall variability of the South–West, while the ENSO is the key driver of rainfall and weather patterns over much of the continent (Risbey *et al* 2009).

5. Extremeness of Australian carbon cycle in 2011

The extremeness of the 2011 carbon-cycle anomaly is quantified in figure 3 by the z-score (number of standard deviations from the local 1982–2013 mean flux). The regionally averaged NPP anomaly was anomalously high (z-score $>$ 1) across all bioclimatic regions, and particularly high ($>$3) in the semi-arid regions. Heterotrophic respiration was similarly elevated across all regions, although less extreme than NPP in the semi-arid regions, leading to particularly elevated NEP (z-score $>$ 3) in these regions and for Australia as a whole. The spatial distributions (figures 3(ii)–(iv)) show the widespread extent of the anomaly.

The spatial pattern of flux anomalies depends not only on the local z-score, but on the local average flux,

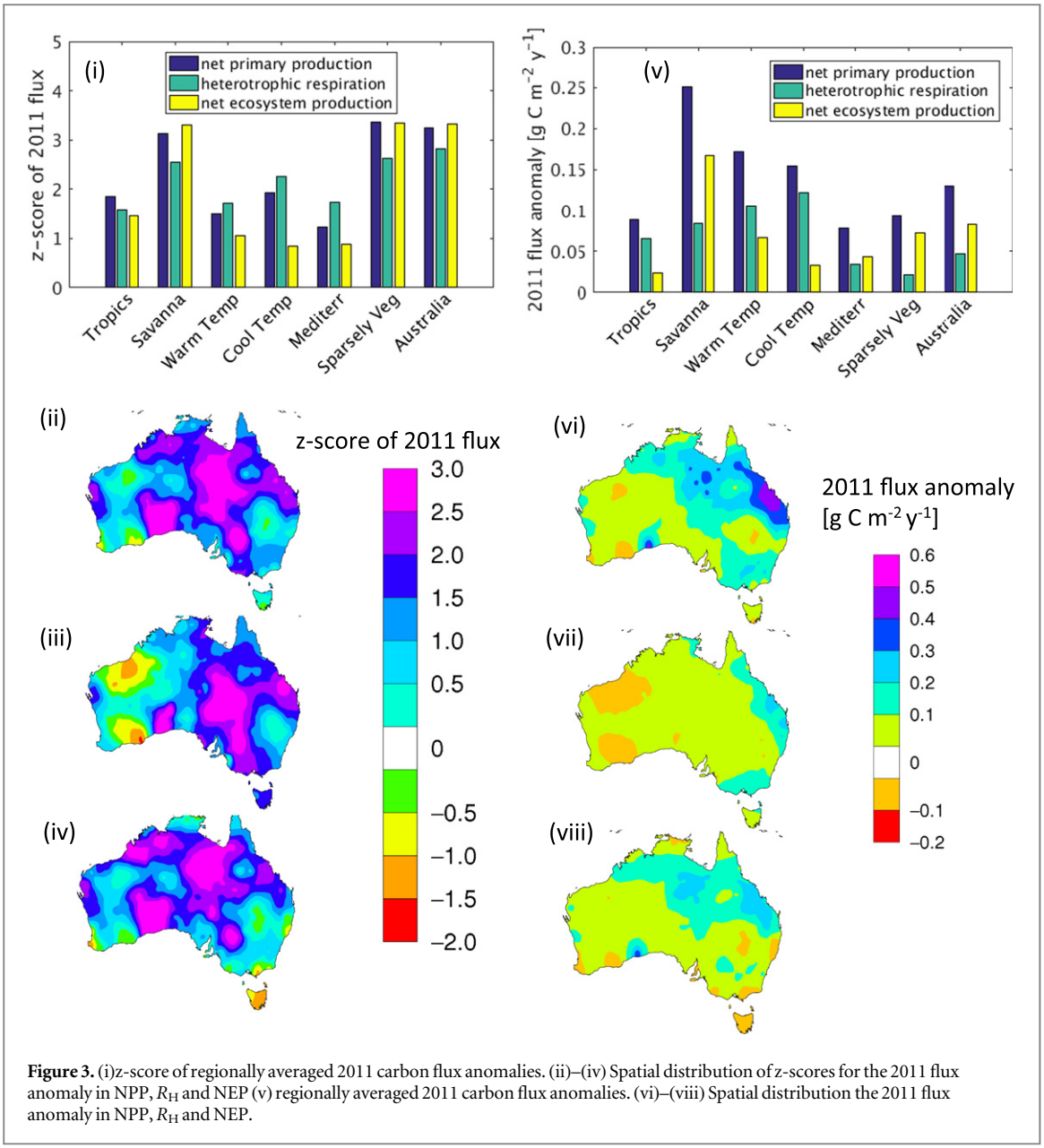

Figure 3. (i)z-score of regionally averaged 2011 carbon flux anomalies. (ii)–(iv) Spatial distribution of z-scores for the 2011 flux anomaly in NPP, R_H and NEP (v) regionally averaged 2011 carbon flux anomalies. (vi)–(viii) Spatial distribution the 2011 flux anomaly in NPP, R_H and NEP.

which differs considerably across the continent. Figures 3(vi)–(viii) reveals that high 2011 NPP flux anomalies occurred in the north-eastern Savanna region, characterised by high productivity and a strong sensitivity of ecosystem functioning to water availability (Raupach *et al* 2013), whereas the NEP flux anomaly was more uniformly spread across the entire Savanna region.

6. Process contributions to IAV in net carbon uptake

Thus far our analysis demonstrates a dampening of interannual variations in continental NEP compared to NPP (figures 1, 2(iv), (vi)) because of temporal correlations between production (NPP) and decomposition (R_H). We now quantify the contributions (equation (3)) of the constituent fluxes (NPP and R_H) to IAV. Figure 4(i) shows the contributions of regional NPP and R_H to continental IAV in NEP. A positive contribution indicates that the constituent flux is correlated with continental NEP, and a negative contribution that it is anti-correlated with continental NEP at the annual time scale. Arrows indicate the sign and magnitude of the relative regional contributions to continental NEP variability. Across all regions, and for the continent as a whole, we see that variations in NPP predominate, but are significantly compensated for by variations in R_H in terms of their contribution to continental NEP variability. R_H variability offsets the contribution of NPP variability by 40% continentally: regionally, the offset is largest in the Savanna region.

The spatial patterns of the NEP and R_H contributions to IAV in NEP (figures 4(ii) and (iii)) reinforce the picture of a dominant contribution by NPP, significantly offset by R_H across most of the continent.

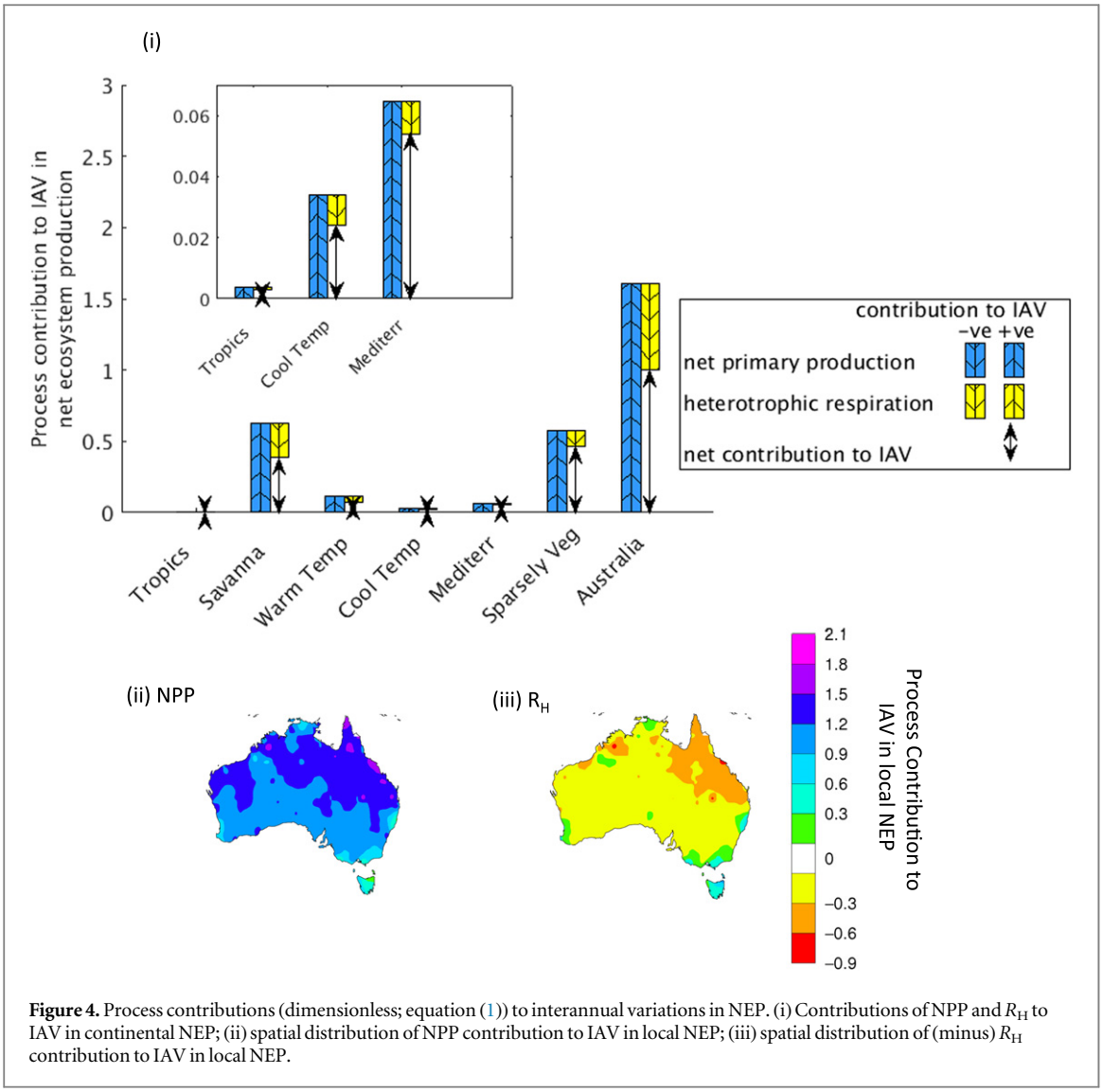

Figure 4. Process contributions (dimensionless; equation (1)) to interannual variations in NEP. (i) Contributions of NPP and R_H to IAV in continental NEP; (ii) spatial distribution of NPP contribution to IAV in local NEP; (iii) spatial distribution of (minus) R_H contribution to IAV in local NEP.

This is because both constituent fluxes respond positively to precipitation anomalies. Parts of the cool temperate regions (Tasmania and Southern Victoria) are exceptional, being characterised by IAV in the R_H component that re-inforces the NPP component (i.e. positive NPP anomalies occur in the same years as negative R_H anomalies).

7. Conclusion

Our results provide a regional assessment, based on best available observational data, of IAV in the Australian terrestrial carbon cycle and the role of Australia in the record land sink anomaly of 2011. Our results fall in line with Ahlström *et al* (2015), Poulter *et al* (2014), Detmers *et al* (2015) and Bastos *et al* (2013), confirming Australia's large role in the record land sink anomaly of 2011. Our results demonstrate that such variability is consistent with a direct physiological response of vegetation productivity to fluctuating water availability, with these interannual variations in productivity being partially offset by a largely correlated opposing effect of fluctuating water availability on decomposition.

Acknowledgments

VH and CMT thank the support of the Australian Climate Change Science Program. BS acknowledges funding as an OCE Distinguished Visiting Scientist to CSIRO Oceans & Atmosphere, Canberra.

References

Ahlström A *et al* 2015 The dominant role of semi-arid ecosystems in the trend and variability of the land CO_2 sink *Science* **348** 895–9

Bastos A, Running S W, Gouveia C and Trigo R M 2013 The global NPP dependence on ENSO: La Niña and the extraordinary year of 2011 *J. Geophys. Res.: Biogeosci.* **118** 1247–55

Detmers R G, Hasekamp O, Aben I, Houweling S, van Leeuwen T T, Butz A, Landgraf J, Köhler P, Guanter L and Poulter B 2015 Anomalous carbon uptake in Australia as seen by GOSAT *Geophys. Res. Lett.* **42** 8177–84

Doherty J E, Hunt R J and Tonkin M J A 2010 Approaches to highly parameterized inversion: a guide to using PEST for model-parameter and predictive-uncertainty analysis *U.S. Geological Survey Scientific Investigations Report* 2010–5211, p 71 (http://pubs.usgs.gov/sir/2010/5211)

Donohue R J, McVicar T R and Roderick M L 2009 Climate-related trends in Australian vegetation cover as inferred from satellite observations, 1981–2006 *Glob. Change Biol.* **15** 1025–39

Haverd V and Cuntz M 2010 Soil–Litter–Iso: a one-dimensional model for coupled transport of heat, water and stable isotopes in soil with a litter layer and root extraction *J. Hydrol.* **388** 438–55

Haverd V, Raupach M R, Briggs P R, Canadell J G, Davis S J, Law R M, Meyer C P, Peters G P, Pickett-Heaps C and Sherman B 2013a The Australian terrestrial carbon budget *Biogeosciences* **10** 851–69

Haverd V, Raupach M R, Briggs P R, Canadell J G, Isaac P, Pickett-Heaps C, Roxburgh S H, van Gorsel E, Viscarra Rossel R A and Wang Z 2013b Multiple observation types reduce uncertainty in Australia's terrestrial carbon and water cycles *Biogeosciences* **10** 2011–40

Haverd V, Smith B, Raupach M, Briggs P, Nieradzik L, Beringer J, Hutley L, Trudinger C M and Cleverly J 2016 Coupling carbon allocation with leaf and root phenology predicts tree–grass partitioning along a savanna rainfall gradient *Biogeosciences* **13** 761–79

Houldcroft C J, Grey W M F, Barnsley M, Taylor C M, Los S O and North P R J 2009 New vegetation Albedo parameters and global fields of soil background albedo derived from MODIS for use in a climate model *J. Hydrometeorol.* **10** 183–98

Hutchinson M F, McIntyre S, Hobbs R J, Stein J L, Garnett S and Kinloch J 2005 Integrating a global agro-climatic classification with bioregional boundaries in Australia *Glob. Ecol. Biogeogr.* **14** 197–212

Isaac P 2014 FluxNet data OzFlux: Australian and New Zealand flux Research and Monitoring hdl: 102.100.100/14247

Le Quéré C *et al* 2015 Global carbon budget 2014 *Earth Syst. Sci. Data* **7** 47–85

Lu H, Raupach M R, McVicar T R and Barrett D J 2003 Decomposition of vegetation cover into woody and herbaceous components using AVHRR NDVI time series *Remote Sens. Environ.* **86** 1–18

Poulter B *et al* 2014 Contribution of semi-arid ecosystems to interannual variability of the global carbon cycle *Nature* **509** 600–3

Raupach M R, Haverd V and Briggs P R 2013 Sensitivities of the Australian terrestrial water and carbon balances to climate change and variability *Agric. Forest Meteorol.* **182–183** 277–91

Risbey J S, Pook M J, McIntosh P C, Wheeler M C and Hendon H H 2009 On the remote drivers of rainfall variability in Australia *Mon. Weather Rev.* **137** 3233–53

Trudinger C M, Haverd V, Briggs P R and Canadell J G 2016 Interannual variability in Australia's terrestrial carbon cycle constrained by multiple observation types *Biogeosciences* accepted

Tucker C J, Pinzon J E, Brown M E, Slayback D A, Pak E W, Mahoney R, Vermote E F and El Saleous N 2005 An extended AVHRR 8 km NDVI dataset compatible with MODIS and SPOT vegetation NDVI data *Int. J. Remote Sens.* **26** 4485–98

van der Werf G R, Randerson J T, Giglio L, Collatz G J, Mu M, Kasibhatla P S, Morton D C, DeFries R S, Jin Y and van Leeuwen T T 2010 Global fire emissions and the contribution of deforestation, savanna, forest, agricultural, and peat fires (1997–2009) *Atmos. Chem. Phys.* **10** 11707–35

Wang W L, Dungan J, Hashimoto H, Michaelis A R, Milesi C, Ichii K and Nemani R R 2011a Diagnosing and assessing uncertainties of terrestrial ecosystem models in a multimodel ensemble experiment: 2. Carbon balance *Glob. Change Biol.* **17** 1367–78

Wang Y P, Kowalczyk E, Leuning R, Abramowitz G, Raupach M R, Pak B, van Gorsel E and Luhar A 2011b Diagnosing errors in a land surface model (CABLE) in the time and frequency domains *J. Geophys. Res.* **116** G01034

Wang Y P, Law R M and Pak B 2010 A global model of carbon, nitrogen and phosphorus cycles for the terrestrial biosphere *Biogeosciences* **7** 2261–82

Zhu Z, Bi J, Pan Y, Ganguly S, Anav A, Xu L, Samanta A, Piao S, Nemani R R and Myneni R B 2013 Global data sets of vegetation leaf area index (LAI) 3g and Fraction of Photosynthetically Active Radiation (FPAR) 3g derived from Global Inventory Modeling and Mapping Studies (GIMMS) Normalized Difference Vegetation Index (NDVI3g) for the period 1981 to 2011 *Remote Sens.* **5** 927–48